C3b deposition on human erythrocytes induces the formation of a membrane skeleton–linked protein complex

Pallop Karnchanaphanurach, … , Anne Nicholson-Weller, David E. Golan

Research Article   Hematology

Decay-accelerating factor (DAF, also known as CD55), a glycosylphosphatidylinositol-linked (GPI-linked) plasma membrane protein, protects autologous cells from complement-mediated damage by inhibiting complement component 3 (C3) activation. An important physical property of GPI-anchored complement regulatory proteins such as DAF is their ability to translate laterally in the plasma membrane. Here, we used single-particle tracking and tether-pulling experiments to measure DAF lateral diffusion, lateral confinement, and membrane skeletal associations in human erythrocyte membranes. In native membranes, most DAF molecules exhibited Brownian lateral diffusion. Fluid-phase complement activation caused deposition of C3b, one of the products of C3 cleavage, onto erythrocyte glycophorin A (GPA). We then determined that DAF, C3b, GPA, and band 3 molecules were laterally immobilized in the membranes of complement-treated cells, and GPA was physically associated with the membrane skeleton. Mass spectrometry analysis further showed that band 3, α-spectrin, β-spectrin, and ankyrin were present in a complex with C3b and GPA in complement-treated cells. C3b deposition was also associated with a substantial increase in erythrocyte membrane stiffness and/or viscosity. We therefore suggest that complement activation stimulates the formation of a membrane skeleton–linked DAF-C3b-GPA–band 3 complex on the erythrocyte surface. This complex may promote the removal of senescent erythrocytes from the circulation.

Find the latest version:

https://jci.me/36088/pdf

C3b deposition on human erythrocytes induces the formation of a membrane skeleton–linked protein complex

Pallop Karnchanaphanurach,[1] Rossen Mirchev,[2] Ionita Ghiran,[3] John M. Asara,[4] Brigitte Papahadjopoulos-Sternberg,[5] Anne Nicholson-Weller,[3] and David E. Golan[2,6]

[1]Department of Chemistry and Chemical Biology, Harvard University, Cambridge, Massachusetts, USA.
[2]Department of Biological Chemistry and Molecular Pharmacology, Harvard Medical School, Boston, Massachusetts, USA.
[3]Department of Medicine and [4]Division of Signal Transduction and Department of Pathology, Beth Israel Deaconess Medical Center and Harvard Medical School, Boston, Massachusetts, USA. [5]NanoAnalytical Laboratory, San Francisco, California, USA.
[6]Hematology Division and Department of Medicine, Brigham and Women's Hospital and Harvard Medical School, Boston, Massachusetts, USA.

Decay-accelerating factor (DAF, also known as CD55), a glycosylphosphatidylinositol-linked (GPI-linked) plasma membrane protein, protects autologous cells from complement-mediated damage by inhibiting complement component 3 (C3) activation. An important physical property of GPI-anchored complement regulatory proteins such as DAF is their ability to translate laterally in the plasma membrane. Here, we used single-particle tracking and tether-pulling experiments to measure DAF lateral diffusion, lateral confinement, and membrane skeletal associations in human erythrocyte membranes. In native membranes, most DAF molecules exhibited Brownian lateral diffusion. Fluid-phase complement activation caused deposition of C3b, one of the products of C3 cleavage, onto erythrocyte glycophorin A (GPA). We then determined that DAF, C3b, GPA, and band 3 molecules were laterally immobilized in the membranes of complement-treated cells, and GPA was physically associated with the membrane skeleton. Mass spectrometry analysis further showed that band 3, α-spectrin, β-spectrin, and ankyrin were present in a complex with C3b and GPA in complement-treated cells. C3b deposition was also associated with a substantial increase in erythrocyte membrane stiffness and/or viscosity. We therefore suggest that complement activation stimulates the formation of a membrane skeleton–linked DAF-C3b-GPA–band 3 complex on the erythrocyte surface. This complex may promote the removal of senescent erythrocytes from the circulation.

Introduction

The complement system is a major effector component of the innate immune response (1). The complement cascade, which involves sequential activation of serum complement proteins, leads to diverse inflammatory effects and, in some cases, lysis of the target. Activation of complement can occur through the classical, alternative, and lectin pathways. All 3 pathways lead to the formation of complement component 3 (C3) convertase, a central enzymatic complement complex that cleaves serum C3 into C3a and C3b. C3b can dock covalently on a membrane surface via amide or ester linkages. Downstream of C3 activation, C3 convertase participates in the formation of C5 convertase, a membrane-bound complex that cleaves serum C5 into C5a and C5b. C5b induces sequential recruitment of complement proteins C6, C7, C8, and C9 to form C5b-9, the terminal complement complex, which creates a pore in the membrane (2).

Normal human cells are protected from homologous complement-mediated damage by the expression of regulatory proteins, such as decay-accelerating factor (DAF), on the extracellular surface of the plasma membrane. DAF is a monomeric 70-kDa glycosylphosphatidylinositol-linked (GPI-linked) glycoprotein, with 4 N-terminal short consensus repeat domains that are linked to the GPI moiety by a heavily glycosylated Ser-Thr-Pro-rich region (3–5). Structural analysis shows that DAF extends 177 Å from the surface of the membrane (6). DAF accelerates the decay of C3 and C5 convertases that form on the autologous membrane, but it does not act on convertases that assemble on adjacent cells (7, 8). DAF-mediated inhibition of C3 and C5 convertases involves binding interactions of DAF with both subunits of the C4b2a classical convertase and both subunits of the C3bBb alternative pathway convertase, leading to decay of the enzymes by dissociation of the catalytic subunits C2a and Bb, respectively (9). The DAF interaction site on each convertase has been mapped (10, 11). Importantly, lower-affinity DAF binding interactions with C4b or C3b have also been documented (12). The latter interactions are critical for surveillance against adventitious deposition of complement in the circulation. The pathological absence of DAF, through a rare genetic deficiency or the more common acquired deficiency in paroxysmal nocturnal hemoglobinuria, results in abnormal C3b deposition on human rbc in vivo (reviewed in ref. 1).
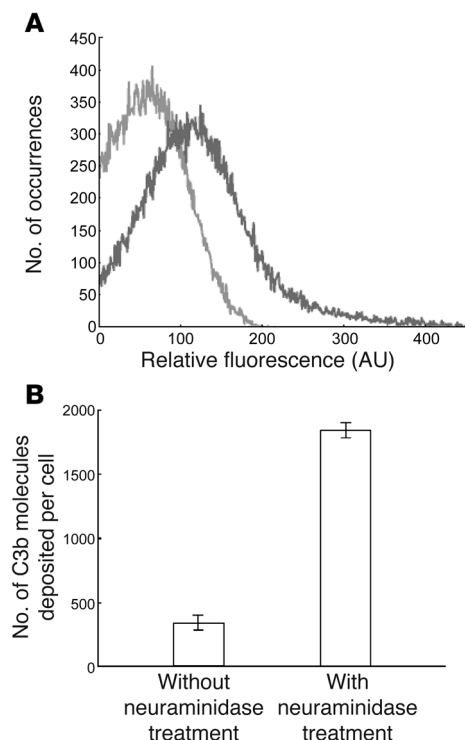
An important physical property of the GPI-anchored complement regulatory proteins is their ability to translate laterally in the plasma membrane. A DAF molecule, for example, would

A

B

Figure 1

C3b deposition on rbc membranes. (**A**) Flow cytometry histogram showing C3b/iC3b deposited on the rbc membrane. Cell-surface C3b/iC3b was labeled using mouse anti-human C3c antibody (dark gray line); labeling with anti-C3dg antibody yielded identical results under the same conditions (data not shown). The sample without primary antibody labeling is shown as a light gray line. The histogram is representative of 2 independent experiments. (**B**) Number of C3b molecules deposited per cell, determined using an ELISA procedure either with or without neuraminidase treatment. Values represent mean ± SD from 3 independent experiments.

not be capable of efficiently locating and deactivating the complement convertases if it were rigidly fixed to 1 membrane site. Nor could it function effectively if its motion prevented it from interacting with newly assembled convertases. In this study, we investigated the lateral mobility of individual DAF molecules in the membrane of intact human rbc, using single particle tracking (SPT), and measured the effect of depositing complement protein C3b on DAF lateral mobility. We found that DAF exhibits free (Brownian) lateral motion in the normal rbc membrane and that DAF mobility becomes tightly confined upon C3b deposition. Using a combination of biochemistry, mass spectrometry, electron microscopy, SPT, and membrane tether-pulling measurements, we show that DAF immobilization results from the formation of a molecular complex involving DAF, C3b, glycophorin A (GPA), and band 3 and that this complex is linked to the underlying spectrin-based membrane skeleton.

Results

Deposition of C3b on the normal rbc membrane. C3b was deposited on normal rbc using purified cobra venom factor (CVF) and C5-depleted human serum. We avoided the use of antibodies to trigger complement activation, since such antibodies could have additional effects on membrane protein dynamics, and we incubated cells for a limited time with C5-depleted human serum to minimize conversion of deposited C3b to hemolytically inactive C3b (iC3b) by plasma factors I and H (13). The presence of C3 fragments on the rbc was verified by flow cytometry (Figure 1A). We found that ELISA more accurately detected C3 antigen when neuraminidase was used to cleave sialic acids from the rbc membrane surface (Figure 1B). Because C3b can covalently attach to GPA via sialic acid (14), it is likely that (a) GPA sterically hinders antibody binding when C3b is probed with 2 antibodies in the ELISA (see Methods) and (b) neuraminidase does not cleave sialic acids that

are bound to C3b. As determined by this modified ELISA, there were 1,840 ± 120 C3b molecules deposited per cell (mean ± SD; $n = 3$ experiments). Using a similar protocol, Ninomiya et al. have estimated that there are 3,110 copies of DAF per normal rbc (15). Under our conditions, therefore, rbc with C3b deposits had about 2 DAF molecules for every C3b molecule deposited on the cell.

DAF exhibits Brownian lateral diffusion in the normal rbc membrane, and C3b deposition specifically induces tight confinement of DAF in the membranes of rbc with C3b deposits. During complement activation, especially via the alternative pathway, the C3b molecules that are generated in large amounts in the plasma can deposit on rbc in the circulation. C3b molecules can also be generated directly on the membranes of normal rbc, as the alternative pathway amplifies de novo complement activation secondary to the binding of antibodies (16). Because DAF is the endogenous regulator of C3b on rbc membranes, we studied whether the diffusion of DAF molecules in the membrane reflects changes caused by C3b deposition. SPT experiments were performed using gold particles functionalized to react specifically with individual molecules of DAF on both normal and C3b-deposited human rbc. The majority (78%) of DAF molecules exhibited Brownian diffusion in the normal rbc membrane (Figure 2A and Figure 3A). The average lateral diffusion coefficient was 41.0×10^{-11} cm^2/s (Table 1). A minor population (22%) of DAF molecules showed a tightly confined mode of lateral motion (Figure 2B and Figure 3A), characterized by an average diffusion coefficient of 4.3×10^{-11} cm^2/s (Table 1).

The majority (72%) of DAF molecules were tightly confined on rbc with C3b deposits, with an average lateral diffusion coefficient of 6.0×10^{-11} cm^2/s (Figure 2D, Figure 3B, and Table 1). A minor population (28%) of DAF molecules showed loosely confined or Brownian diffusion (see Methods) in rbc with C3b deposits, with an average diffusion coefficient of 50.0×10^{-11} cm^2/s (Figure 2C, Figure 3B, and Table 1). Therefore, C3b deposition immobilized 50% (i.e., 72%–22%) of the DAF molecules on the rbc membrane.

To test whether the effect of C3b deposition on DAF mobility was specific for DAF and not a global effect on all rbc membrane proteins, we also studied the diffusion of CD58 (lymphocyte function-associated antigen 3), a GPI-linked membrane protein that is not involved in complement regulation. CD58 has an apparent molecular weight of 55 to 70 kDa, similar to that of DAF, and there are about 5,000 copies of CD58 per normal rbc (17). However, in contrast to its effects on DAF mobility, C3b deposition had no significant effect on the lateral mobility of CD58. Specifically, C3b did not alter the ratio of confined and Brownian CD58 subpopulations (Figure 3, C and D, and Table 1), and C3b did not affect the CD58 time-dependence factor value (α; $P = 0.48$), diffusion coefficient (D; $P = 0.91$), or radius of con-
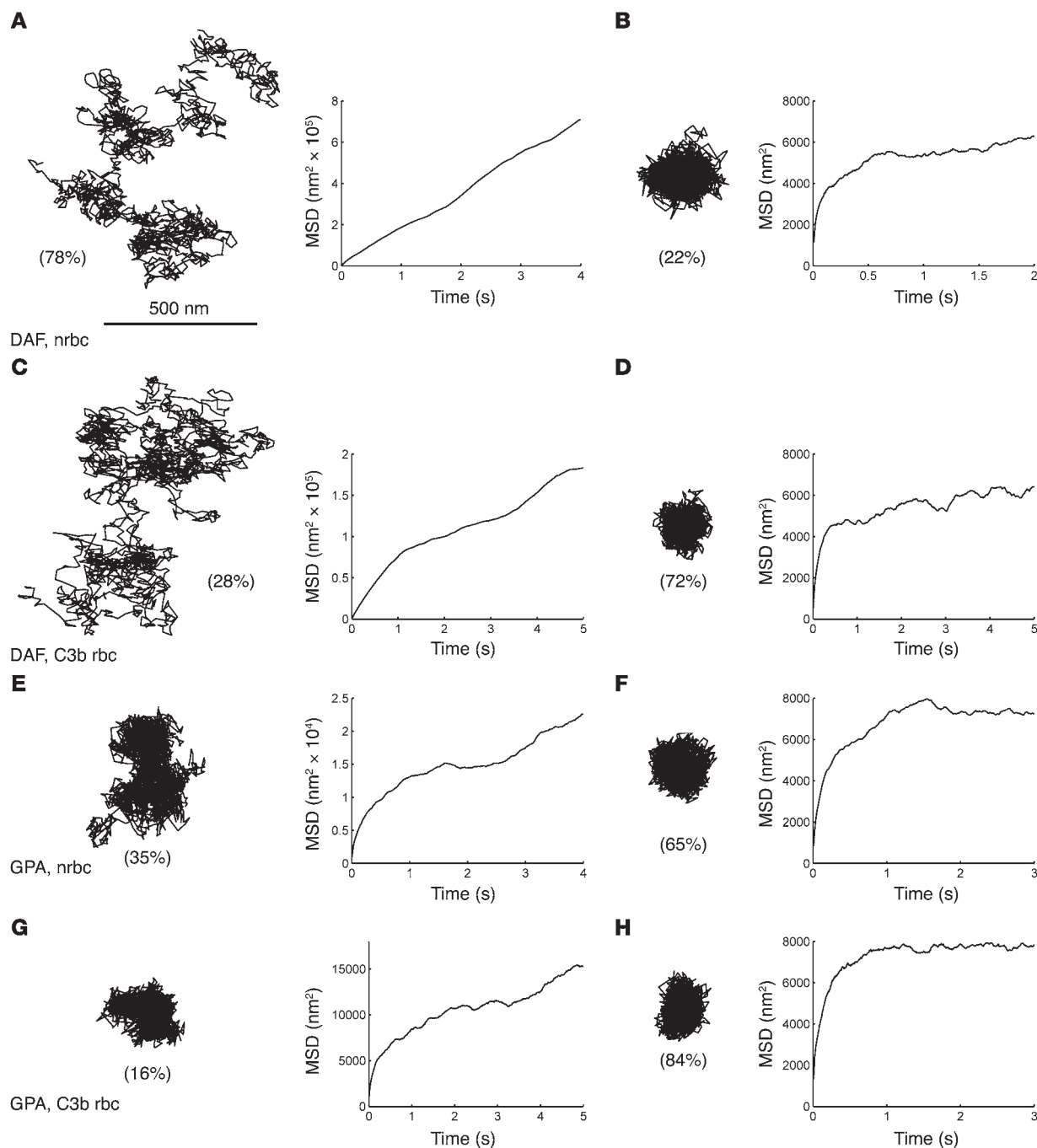
Figure 2
Representative SPT trajectories of DAF and GPA lateral diffusion in membranes of normal rbc (nrbc) and rbc with C3b deposits (C3b rbc). Each step in a trajectory represents the displacement of an individual gold-labeled molecule over a 33-millisecond time interval. The graphs show the initial MSD versus Δt profiles of the respective trajectories. (**A**) The majority of DAF molecules (78%) exhibit Brownian diffusion in normal rbc. (**B**) A minor population of DAF molecules (22%) shows tightly confined motion in normal rbc. (**C**) A minor population of DAF molecules (28%) exhibits loosely confined diffusion in rbc with C3b deposits. (**D**) The majority of DAF molecules (72%) show tightly confined motion in rbc with C3b deposits. (**E**) A minor population of GPA molecules (35%) exhibits loosely confined diffusion in normal rbc. (**F**) The majority of GPA molecules (65%) show tightly confined motion in normal rbc. (**G**) A minor population of GPA molecules (16%) exhibits loosely confined diffusion in rbc with C3b deposits. (**H**) The vast majority of GPA molecules (84%) show tightly confined motion in rbc with C3b deposits. The scale is the same for all SPT trajectories (scale bar: 500 nm). Note that the range of the *y* axis (MSD) values is substantially greater for the randomly diffusing molecules (**A** and **C**) than for the confined molecules.
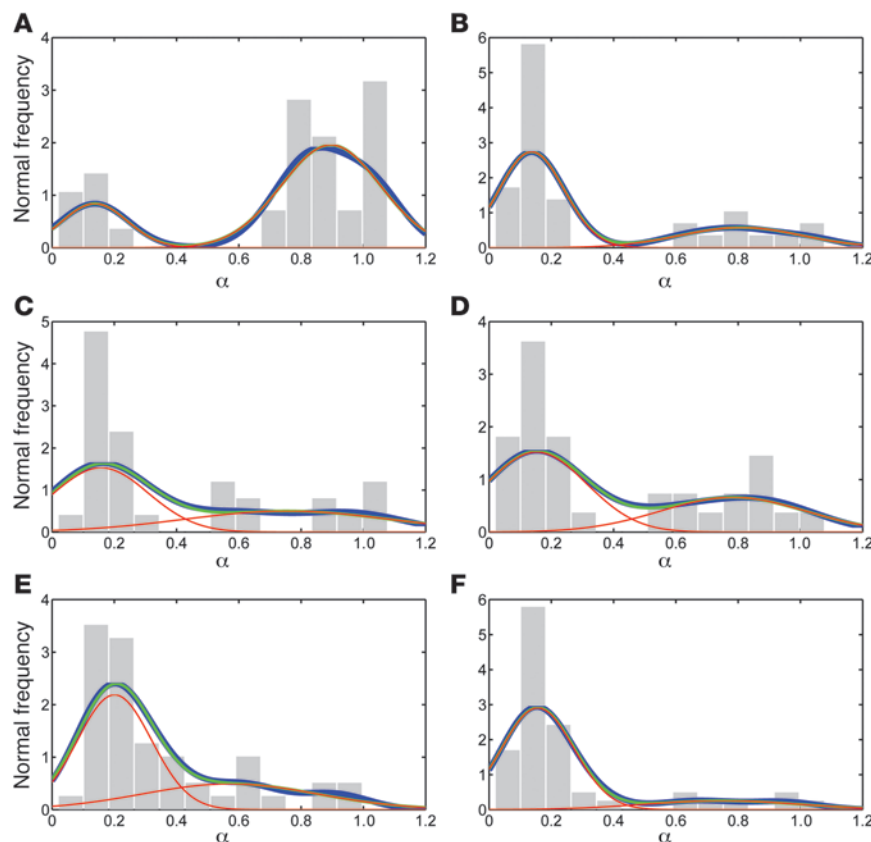
Figure 3
Distribution of time-dependence factor values for trajectories of motion of DAF, CD58, and GPA in membranes of normal rbc and rbc with C3b deposits. (**A**) DAF in normal rbc. (**B**) DAF in rbc with C3b deposits. (**C**) CD58 in normal rbc. (**D**) CD58 in rbc with C3b deposits. (**E**) GPA in normal rbc. (**F**) GPA in rbc with C3b deposits. In each graph, the gray bars represent a histogram of the experimental data; the blue curves represent the envelope smoothing function calculated from the experimental data; the red curves are Gaussian best-fit distributions, describing the 2 deconvolved populations; and the green curves are the sum of the 2 red curves (see Methods). In all of the panels, the 2 red curves are normal distributions that differ statistically from one another, according to Equation 2. Trajectories with time-dependence factor (α) values falling under the Gaussian curve, with the lower mean in each graph, are classified as tightly confined (mean α, 0.14–0.20), and trajectories with time-dependence factor values falling under the Gaussian curve, with the higher mean in each graph, are classified as loosely confined or Brownian (mean α, 0.57–0.90). Based on these distributions, we used an time-dependence factor value of 0.4 as the cutoff between the population of tightly confined trajectories ($\alpha \le 0.4$) and the population of loosely confined or Brownian trajectories ($\alpha > 0.4$).

finement (r_c; P = 0.87). These results suggested that the immobilization of DAF by C3b was caused by a specific binding interaction between C3b and DAF.

C3b binds GPA on normal rbc, and the diffusion behavior of tightly confined DAF is similar to that of GPA in the membranes of rbc with C3b deposits. Using radioimmunoblots, Parker and colleagues reported that C3b binds preferentially to sialic acid moieties on GPA, on both paroxysmal nocturnal hemoglobinuria and normal human rbc (14). Here, coimmunoprecipitation experiments indicated that C3b and GPA were coprecipitated in a high-molecular-weight complex (Figure 4), confirming the results of Parker and colleagues (14). As a control, the presence of EDTA inhibited both C3b deposition and the shift of GPA into the high-molecular-weight complex.

The binding of C3b to GPA suggested that DAF, which also binds to C3b, could become linked to GPA in a ternary DAF-C3b-GPA complex on rbc with C3b deposits. We therefore hypothesized that the lateral diffusion of tightly confined DAF molecules would be similar to that of a fraction of GPA molecules on rbc with C3b deposits. To test this hypothesis, we used SPT to measure the lateral mobility of GPA on rbc with C3b deposits. We first derivatized cell-surface GPA with fluorescein thiosemicarbazide and then labeled the fluorescein with anti-fluorescein–coated gold particles in order to avoid potential secondary effects of ligating GPA directly with anti-GPA antibodies (see below). The major fraction of GPA showed tightly confined diffusion on rbc with C3b deposits, and the parameters (α, D, and r_c) characterizing the lateral diffusion of tightly confined DAF molecules were similar to those characterizing the diffusion of tightly confined GPA molecules (Figure 2, F and H, Figure 3, E and F, and Table 1). These results represented only a partial test of our hypothesis, because rbc with C3b deposits contained GPA (about 250,000 dimers) in great excess of C3b (1,840 molecules). Nonetheless, the results were consistent with a model in which DAF is tightly confined in rbc with C3b deposits by physical association with tightly confined GPA molecules (see Discussion).

Membrane skeletal attachment of GPA is increased in the membranes of rbc with C3b deposits. Based on these results, we hypothesized that the confinement of DAF on rbc with C3b deposits was due to formation of a stable complex containing DAF, C3b, and GPA. Chasis and colleagues have studied the molecular interactions that cause GPA immobilization in the rbc membrane (18–20). Specifically, these investigators have shown that several anti-GPA antibodies alter the conformation of GPA in human rbc. As measured by ektacytometry and integral protein lateral mobility, antibody binding to different epitopes on the extracellular domain of GPA induces varying degrees of membrane skeletal attachment of the molecule. It therefore seemed likely that GPA could undergo a similar change upon interaction with C3b and DAF.

We used laser optical tweezers (LOT) to study the putative attachment of GPA to the membrane skeleton in normal rbc and rbc with C3b deposits. Thin lipid tethers could be pulled from the membrane if the bead-labeled receptor was not linked to the membrane skeleton. In contrast, tether formation was prevented if the bead-labeled receptor was attached to the membrane skeleton (Figure 5, A and B; see Methods). This technique was therefore capable of distinguishing between 2 states of membrane interaction of a cell surface protein: (a) protein-lipid association and (b) protein

Table 1
Diffusion of DAF, CD58, GPA, and band 3 in normal rbc and membranes of rbc with C3b deposits

rbc	Protein	Tightly confined diffusion				Loosely confined or Brownian diffusion		
		α	D $(10^{-11}$ cm^2/s)	r_c (nm)	Fraction of trajectories	α	D $(10^{-11}$ cm^2/s)	Fraction of trajectories
Normal	DAF	0.14 ± 0.10	4.3 ± 1.4	80 ± 20	22%	0.90 ± 0.20	41.0 ± 22.0	78%
	CD58	0.16 ± 0.15	6.2 ± 2.4	104 ± 24	58%	0.75 ± 0.33	17.0 ± 16.0	42%
	GPA	0.20 ± 0.10	2.1 ± 0.8	63 ± 12	65%	0.57 ± 0.28	2.7 ± 2.7	35%
	Band 3, pop. 1	0.14 ± 0.06	5.8 ± 3.5	98 ± 29	25%–50%			
	Band 3, pop. 2	0.29 ± 0.11	18.0 ± 4.5	174 ± 8	50%–75%			
C3b-deposited	DAF	0.14 ± 0.10	6.0 ± 2.6	89 ± 20	72%	0.81 ± 0.20	50.0 ± 37.0	28%
	CD58	0.15 ± 0.16	6.0 ± 1.6	100 ± 14	61%	0.78 ± 0.23	15.0 ± 7.0	39%
	GPA	0.16 ± 0.10	2.8 ± 1.2	66 ± 15	84%	0.75 ± 0.25	3.1 ± 2.1	16%
	Band 3, pop. 1	0.15 ± 0.05	6.5 ± 1.8	110 ± 5	44%			
	Band 3, pop. 2	0.28 ± 0.13	6.5 ± 1.8	110 ± 5	56%			

α, time-dependence factor; D, diffusion coefficient; r_c, radius of confinement; pop., population. Values represent mean ± SD.

attachment to the membrane skeleton. Care was taken to ensure that a minimal amount of antibody was used for polystyrene bead conjugation and to establish the optimal tether-pulling rate, trap stiffness, and relative positions of bead and cell. In normal rbc, we found that a fine lipid tether was formed for 80% ± 7% (mean ± SD) of DAF molecules, whereas 38% ± 4% of GPA molecules allowed the formation of lipid tethers (Figure 5C). Both DAF and GPA became substantially more membrane skeleton–bound on rbc with C3b deposits (55% ± 5% and 96% ± 4%, respectively; Figure 5C), suggesting that C3b deposition induced attachment of the DAF-C3b-GPA complex to the membrane skeleton.

Mass spectrometry analysis suggests that C3b deposition induces the formation of GPA–band 3 complexes linked to the spectrin-based membrane skeleton via ankyrin. We next sought to determine the molecular mechanism by which C3b deposition increased the association of GPA with the membrane skeleton. In normal rbc, a fraction of GPA molecules are bound to band 3 tetramers that are linked to ankyrin. In turn, the band 3–linked ankyrin molecules are attached to the spectrin heterotetramers that connect the actin-based junctional complexes of the erythrocyte membrane skeleton (21). We used microcapillary liquid chromatography, tandem mass spectrometry to perform an analysis of the high-molecular-weight complex associated with GPA in rbc with C3b deposits (see Methods). The only erythroid peptides found in this analysis corresponded to band 3, ankyrin, α-spectrin, and β-spectrin (Table 2 and Supplemental Table 1). The high-molecular-weight complex, immunoprecipitated using anti-C3b antibody, also contained GPA by immunoblot (Figure 4); our failure to detect GPA by mass spectrometry likely resulted from the fact that GPA is highly glycosylated and difficult to digest with trypsin (22). Mass spectrometry analysis showed that complement proteins C3 and C4 (Table 2) and human Ig (Supplemental Table 1) were also associated with the GPA-containing high-molecular-weight complex; the deposition of Ig and C4 may have been an epiphenomenon that occurred after the primary deposition of C3b on GPA (see Discussion). Together, these results strongly suggested that C3b deposition induced the formation of GPA–band 3 complexes linked to the spectrin-based membrane skeleton via ankyrin.

Diffusion of band 3 is decreased in the membranes of rbc with C3b deposits. Based on the results of the mass spectrometry analysis, we hypothesized that band 3 was involved in the molecular mechanism by

which GPA was immobilized in rbc with C3b deposits. We tested this hypothesis by using SPT to measure the lateral mobility of band 3 in normal rbc and rbc with C3b deposits. Band 3 exists in 2 populations in normal rbc: the first fraction consists of laterally immobile ankyrin-linked band 3 homotetramers, and the second fraction consists of laterally mobile band 3 homodimers. Here, 2 populations of band 3 molecules could be distinguished by SPT in normal rbc. In the first population, 25%–50% of band 3 molecules exhibited tightly confined diffusion (α = 0.14 ± 0.06; r_c = 98 ± 7 nm), with an average lateral diffusion coefficient of 5.8×10^{-11} cm^2/s. In the second population, 50%–75% of band 3 molecules showed less tightly confined diffusion (α = 0.29 ± 0.11; r_c = 174 ± 8 nm), with an average diffusion coefficient of 18.0×10^{-11} cm^2/s (Figure 6, A–C, and Table 1). C3b deposition caused a marked shift in these populations: 100% of band 3 molecules exhibited increased confinement (r_c = 110 ± 5 nm) and slow diffusion (D = 6.5×10^{-11} cm^2/s), and the distribution of time-dependence factor values was shifted toward tighter confinement (44%, α = 0.15 ± 0.05; 56%, α = 0.28 ± 0.13) (Figure 6, D–F, and Table 1). These results suggested that C3b deposition caused increased association of band 3 with the membrane skeleton and that the C3b-induced DAF-C3b-GPA complex could be immobilized through binding to ankyrin-linked band 3 homotetramers.

Intramembrane particles are increased in size in the membranes of rbc with C3b deposits. Mass spectrometry, SPT, and LOT measurements all suggested that C3b deposition induced an increase in the degree of association of GPA–band 3 complexes with the rbc membrane skeleton. We used freeze-fracture electron microscopy (FFEM) to estimate the size and degree of clustering of band 3–containing intramembrane particles (IMPs) (23) in normal rbc and rbc with C3b deposits. After C3b deposition, cells were preserved by gentle fixation with 0.5% glutaraldehyde for 30 minutes at 0°C. This mild fixation step did not alter the discocytic morphology of either normal rbc or rbc with C3b deposits. Interestingly, rbc with C3b deposits (but not normal rbc) became echinocytic upon fixation with higher concentrations of glutaraldehyde or longer incubation times, again suggesting that C3b deposition increased the degree of coupling between the rbc membrane bilayer and the membrane skeleton (data not shown). In normal rbc, the IMPs were homogeneously distributed and covered 19% of the membrane surface (Figure 7A); these results were in good agreement
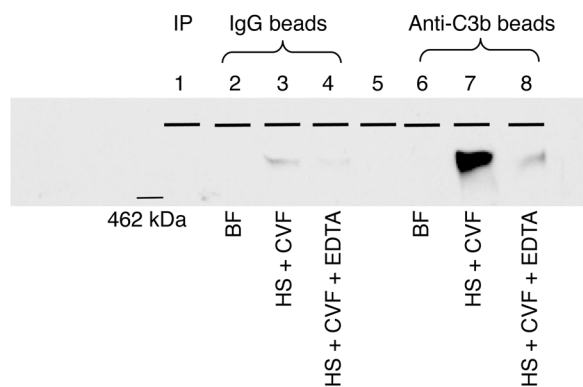
Figure 4
Coimmunoprecipitation of C3b and GPA. rbc were incubated with buffer alone (lanes 2 and 6), C5-depleted human serum and CVF (lanes 3 and 7), or C5-depleted human serum, CVF, and EDTA (lanes 4 and 8). The rbc were then lysed and centrifuged, and the supernatant was immunoprecipitated with agarose beads coupled to isotype-control antibody (IgG; lanes 2–4) or anti-C3b monoclonal antibody (anti-C3b; lanes 6–8). The beads were washed and boiled in Laemmli nonreducing loading buffer, and proteins were separated on 2 identical 3%–8% Tris-Acetate gels. Proteins from the first gel were transferred onto nitrocellulose paper and developed with anti-GPA monoclonal antibody. The molecular weight of the GPA-positive band (lane 7) was greater than that of the 462-kDa standard of the prestained high-molecular-weight standard (lane 1). The second gel was used for mass spectrometry analysis of the C3b-GPA complex (see Table 2). BF, buffer; HS, C5-depleted human serum.

with earlier reports (24). The IMPs were also homogeneous in size, with an average IMP area of about 100 nm² and a narrow distribution of IMP area values (Figure 7C). In contrast, a fraction of much larger IMPs was observed in rbc with C3b deposits (Figure 7, B and C). The inset of Figure 7C shows the cumulative density functions of the 2 IMP area distributions; this analysis indicated that about 40% of the IMPs in rbc with C3b deposits were outside the range of IMP areas found in normal rbc. The IMPs covered about 15% of the membrane surface in rbc with C3b deposits (Figure 7B).

Shape recovery time is prolonged in the membranes of rbc with C3b deposits. C3b-induced alterations in the coupling between transmembrane proteins (GPA and band 3) and membrane skeletal proteins (spectrin and ankyrin) could affect the viscoelastic properties of the rbc membrane, and previous investigators have shown that deposition of C3b on Ig-coated rbc via the alternative pathway of complement activation causes the rbc to become less deformable (25). Here, we activated complement in the fluid phase, using the alternative pathway activator CVF, and we used the time required for recovery of cell shape after mechanical deformation as a measure of rbc viscoelastic properties. We employed LOT to deform individual erythrocytes, and we measured the time required to recover the original discocytic shape after switching off the laser tweezers. In agreement with the results of Sung et al. (25), a significant difference was observed between the shape recovery time in normal rbc (102 ± 2 ms) and that in rbc with C3b deposits (117 ± 3 ms) (Figure 8; $P = 0.0001$). Assuming that the shear elastic modulus of the membrane did not change with C3b deposition (26–28), a longer shape recovery time most likely indicated increased membrane viscosity in the rbc with C3b deposits.

Discussion

Complement activation is greatly amplified at the step of C3b generation, and it is not surprising that several fluid-phase and membrane complement regulators act at this step. One of the membrane complement inhibitors, DAF, has an important role in regulating C3 activation on the autologous cell membrane. In this report, we have examined the effect of C3b deposition on the lateral diffusion of DAF in human rbc membranes. Our results indicate that DAF becomes laterally confined on rbc with C3b deposits, and that this lateral confinement is due to formation of a DAF-C3b-GPA–band 3 complex. We also show that formation of this complex induces a marked increase in the membrane skeletal attachment of GPA and band 3. A model based on these results is presented in Figure 9.

There are relatively few DAF molecules on each human rbc, and the ability of DAF to diffuse laterally in the rbc membrane is likely to be important for its function as a complement regulator. Rapid diffusion of DAF is enabled by its GPI linkage, which extends only into the outer leaflet of the membrane bilayer. When the function of a transmembrane DAF construct (DAF-TM) was compared with that of GPI-anchored DAF in transfected CHO cells, no significant difference was found in the level of protection from cytotoxicity by the 2 DAF isoforms (29). The proposed explanations were that either (i) the lateral mobility of DAF was not an important determinant of its function as a complement regulator or (ii) GPI-linked DAF and DAF-TM had similar lateral mobilities. Other investigators have demonstrated, however, that a transfected, GPI-linked membrane protein isoform showed enhanced lateral mobility compared with the transfected transmembrane isoform of the same protein (30). In addition, there are at least 2 plausible explanations for the lack of a difference in the function of GPI-linked DAF and DAF-TM in the studies using CHO cells (29). First, the CHO cell assay involved C5b-9–dependent cytotoxicity, which is an indirect measure of C3b function; thus, the assay may not have been sufficiently sensitive to measure the effect of DAF lateral mobility differences on C3b function. Second, the transfected CHO cells likely expressed substantially more DAF protein than normal cells, especially rbc, and a relative excess of GPI-linked DAF or DAF-TM could compensate for differences in their lateral mobility. It seems intuitive that a relatively sparse protein, such as DAF on rbc, would require high lateral mobility in order to control complement activation over a relatively large region of membrane, but further studies are needed to determine whether the lateral mobility of DAF depends on its GPI anchor.

A minor population of DAF molecules is tightly confined in the normal rbc membrane. This degree of confinement may reflect the interaction of DAF with small amounts of endogenously generated C3b. The ability of C3b deposition in vitro to increase the fraction of tightly confined DAF molecules supports this argument. The lack of effect of C3b deposition on CD58 mobility suggests that DAF is *specifically* confined when it is bound to C3b. The fact that DAF remains confined for at least 20 seconds on rbc with C3b deposits indicates that an individual DAF molecule could be committed to its regulatory action at a single site of complement activation. Furthermore, the prolonged nature of the confinement suggests that the binding avidity between DAF and C3b is very high on the rbc membrane surface. The apparent association constant for solution-phase
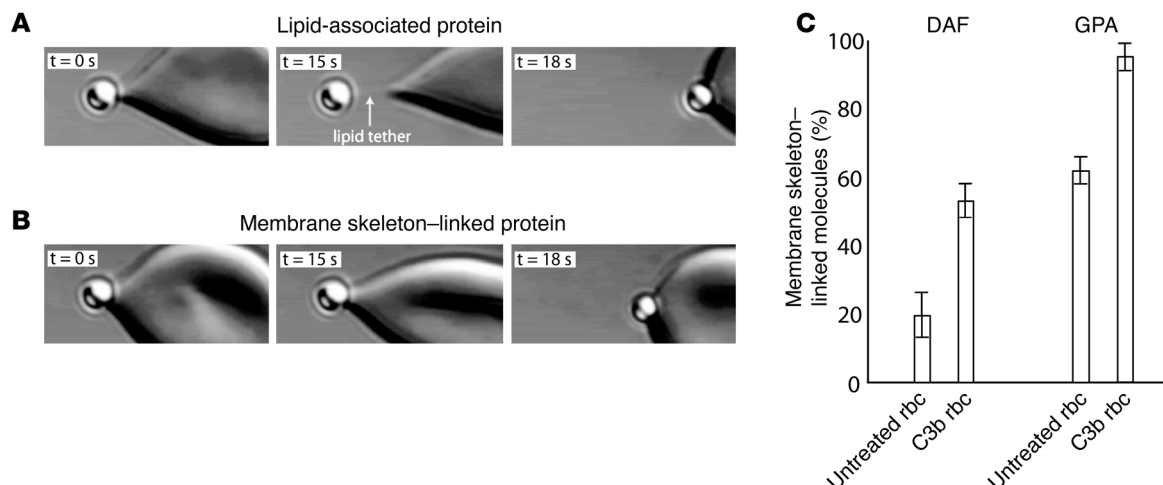
Figure 5
Use of tether-pulling experiments to probe the linkage of membrane proteins to the underlying rbc membrane skeleton. A 1-μm polystyrene bead was covalently attached to monoclonal antibody directed against DAF or GPA. The LOT were used to trap and gradually pull the bead away from the rbc with constant velocity. (**A**) If the bead is attached to a lipid-associated protein, a fine lipid tether is formed. (**B**) However, if the labeled protein is membrane skeleton linked, then the bead remains bound to the cell. Original magnification, ×200 (**A** and **B**). This technique was used to discern the type of membrane interaction for DAF and GPA. (**C**) The membrane skeleton–linked fractions of DAF and GPA are shown for normal (untreated) rbc and rbc with C3b deposits. Error bars represent SD from 3 independent sets of tether-pulling experiments, in which each set of experiments contained 20 individual tether-pulling observations.

binding between DAF and C3b is only 45 nM^{-1} (31), supporting the notion that the 2-dimensional membrane environment substantially enhances DAF functionality.

Our estimate for the number of C3b molecules deposited per rbc (1,840 or about 59% of the 3,110 DAF molecules per rbc) is in agreement with the SPT data, which suggest that an additional 50% of DAF molecules become tightly confined upon C3b deposition (Table 1). This result also suggests a one-to-one binding interaction between DAF and C3b, which is consistent with the recently solved structure of DAF (6). Furthermore, our findings are consistent with an earlier biochemical approach that was able to detect C3b-DAF complexes in the rbc membrane, but only after chemical crosslinking, suggesting that the binding was reversible (12).

The diffusion properties of tightly confined DAF molecules are similar to those of tightly confined GPA molecules on rbc with C3b deposits, supporting the model that DAF is laterally confined via complex formation with C3b-bound GPA. The increased immobilization of GPA, upon C3b deposition, could in turn be caused by its increased interaction with band 3 and with the underlying membrane skeleton. The radius of GPA confinement could represent the amplitude of oscillation of a bound GPA molecule about its band 3/ankyrin attachment point or it could be governed by steric interactions between the cytoplasmic domain of GPA and the membrane skeleton. The observations that confined GPA molecules remain within the same confinement area for the entire observation period (20 seconds) and that nearly 100% of GPA molecules are linked to the membrane skeleton in rbc with C3b deposits suggest that the dominant mode of confinement is a binding, rather than a steric, interaction among GPA and one or more proteins of the rbc membrane (most likely, band 3) and membrane skeleton.

The band 3 molecules in the C3b-induced protein complex could be either the membrane skeleton–linked band 3 homotetramers or the more mobile band 3 homodimers. To address this issue,

we measured the lateral mobility of band 3 in normal rbc and rbc with C3b deposits. In normal rbc, we observed 2 populations of band 3 molecules that differed by their average diffusion coefficient and degree of confinement. In rbc with C3b deposits, an increased fraction of band 3 molecules was in the tightly confined population and all the band 3 molecules exhibited diffusion coefficients characteristic of the slowly diffusing population. We also used FFEM to visualize the size and degree of clustering of IMPs (which consist mainly of band 3 and associated molecules) in rbc with C3b deposits and normal rbc. A fraction of IMPs in rbc with C3b deposits were substantially larger than the IMPs in normal rbc, but the fraction of membrane surface area occupied by IMPs was similar in rbc with C3b deposits and normal rbc. Furthermore, we saw no linear band 3 oligomers similar to those observed in Southeast Asian ovalocytosis rbc (23). These results suggested that the band 3 immobilization observed in rbc with C3b deposits was due to increased binding to the membrane skeleton, rather than crowding of proteins in the membrane.

As described by Chasis and colleagues (18–20), antibody binding to the extracellular domain of GPA induces immobilization of the receptor and rigidification of the normal human rbc membrane. A relatively low concentration of anti-GPA monoclonal antibody (5 μg/ml 9A3, IgG) reduces rbc deformability by 1.7-fold, and a saturating concentration of antibody (40 μg/ml) reduces deformability by 4.5-fold (18–20). In contrast, rbc containing mutant GPA molecules that lack the cytoplasmic domain of GPA do not show immobilization and membrane stiffening upon antibody binding. Furthermore, anti-GPA antibodies induce immobilization of a second integral rbc membrane protein, band 3, in addition to GPA (20). The cooperative effect of antibody binding on the skeletal interactions of these 2 abundantly expressed rbc membrane proteins suggests that GPA ligation by C3b could have wide-ranging consequences for rbc membrane structure and function. Our SPT experiments show that deposition of 1,840 C3b

Table 2
Complement and rbc proteins identified in the high-molecular-weight complex containing GPA[A]

Protein name	Swiss-Prot accession I.D.	Protein identification probability (%)	aa sequence coverage (%)	No. peptides
C3	C03_human	100	32.70	33
C4	C04A_human, C04B_human	99.5	2.18	2
Band 3 (CD233)	B3AT_human	99.9	6.92	3
Ankyrin-1	ANK1_human	100	0.15	6
Spectrin β chain, erythroid	SPTB1_human	100	0.39	13
Spectrin α chain, erythroid	SPT_human	100	0.80	50

[A]Complement was deposited on normal rbc using purified CVF and C5-depleted human serum. SDS-PAGE showed the formation of a high-molecular-weight protein complex with molecular weight of more than 462 kDa. This complex was excised from the gel, digested with trypsin, and sequenced by liquid chromatography, tandem mass spectrometry. Proteins were identified by searching fragmentation data against the reversed Swiss-Prot database.

molecules caused a 19% increase in the number of confined GPA molecules and a 19% increase in the number of confined band 3 molecules (Table 1). Assuming that there are 250,000 GPA dimers and 100,000–250,000 band 3 tetramers per rbc (32), this means that about 47,500 GPA dimers and up to 47,500 band 3 tetramers underwent immobilization upon the binding of only 1,840 C3b molecules. Similarly, tether-pulling experiments revealed that about 34% of GPA molecules, or about 85,000 GPA dimers, become attached to the membrane skeleton upon the deposition of 1,840 C3b molecules.

We hypothesize that C3b is a natural ligand for GPA, and that the interaction of GPA with moderate amounts of C3b results in the same GPA immobilization and membrane stiffening as that induced by limited antibody ligation of GPA. In vitro, oligomers of GPA are known to form when IgM cold-reacting antibodies trigger complement activation (33). Other membrane proteins may also be affected when C3b is deposited; for example, Craig et al. reported an altered distribution of complement receptor 1 (CR1) in the rbc membrane (34). Together, the SPT and tether-pulling results suggest that the effect of a relatively small number of C3b molecules on GPA and band 3 mobility is amplified by another mechanism. For example, long-range effects could be transduced by a global change in the linkages, involving the membrane skeletal proteins and their transmembrane protein attachments (e.g., band 3). Indeed, mass spectrometry analysis of the C3b-associated protein complex in the membranes of rbc with C3b deposits confirmed that not only band 3 but also the membrane skeletal proteins spectrin and ankyrin were involved in the immobilization. Thus, our results provide evidence for a molecular mechanism that relates complement activation to global changes in rbc membrane organization.

We also measured the effect of C3b deposition on the time of shape recovery after extensional deformation of the cell. Shape recovery time is a reliable measure of the viscoelastic properties of the cell. The characteristic time constant (t_c) is obtained by dividing membrane viscosity (η) by the shear elastic modulus (μ): $t_c = \eta/\mu$ (27). This equation suggests that shape recovery is driven by the elastic energy stored in the membrane and is opposed by viscous dissipation. The relaxation time constant is measured by performing an exponential fit of the extended cell length versus time curve. Normal rbc typically show an average time constant value of 100 milliseconds (27, 35), although values up to 300 milliseconds have been reported, depending on the technique used to perform the measurement (36–39). The

shape recovery time in senescent rbc is 20%–50% longer than in young rbc (26, 40). Since an independent measurement of the shear elastic modulus has shown no dependence on cell age (40), it has been proposed that the membrane viscosity value is increased in senescent rbc. Our time constant values in normal rbc are in good agreement with previous reports, and we found a substantial increase in time constant in rbc with C3b deposits compared with normal rbc. It is therefore likely that rbc with C3b deposits are less deformable than normal rbc.

One possible consequence of C3b-induced changes in rbc membrane viscoelastic properties could be the removal of rbc with C3b deposits in the liver or spleen. Senescent rbc are phagocytosed by resident macrophages in these organs, and the clearance of senescent rbc is thought to take place through a series of events that change the antigenic and/or physical properties of the rbc membrane (41). Mechanisms proposed to explain the selective recognition of senescent rbc by macrophages include desialylation of membrane proteins (42), oxidative damage (43), the presence of phosphatidylserine in the outer leaflet of the rbc membrane (44, 45), and band 3 clustering with increased deposition of autologous Ig (46–48). Furthermore, a subclass of IgG, with specificity for a neoantigen on clustered band 3, is able to assemble an alternative complement pathway convertase that amplifies C3b deposition (49). rbc must pass through small fenestrations in the spleen, and a decrease in rbc membrane deformability could be a determinant for the recognition of senescent rbc by splenic macrophages (40). Because rbc aging is associated with increased deposition of C3b (50), we speculate that the formation of the DAF-C3b-GPA–band 3 complex induces increased coupling between the membrane skeleton and the lipid bilayer as well as increased membrane viscosity, thereby enhancing macrophage recognition of the less deformable, senescent rbc.

Methods

Buffers and reagents

Colloidal gold (40 nm in diameter) was from Research Diagnostics. HEPES buffer was from Mediatech. Purified CVF and C5-depleted human serum were from Quidel. Gelatin-Veronal buffer (GVB++), nickel (II) chloride hexahydrate, glucose, sodium phosphate (monobasic and dibasic forms), sodium chloride, potassium chloride, BSA, Triton X-100, 2-(N-morpholino) ethanesulfonic acid (MES) buffer, N-hydroxysuccinimide, 1-ethyl-3-(3-dimethylaminopropyl) carbodiimide hydrochloride, ethanolamine, calcium chloride, sucrose, $C_{12}E_8$, and *Vibrio cholerae* neuraminidase were
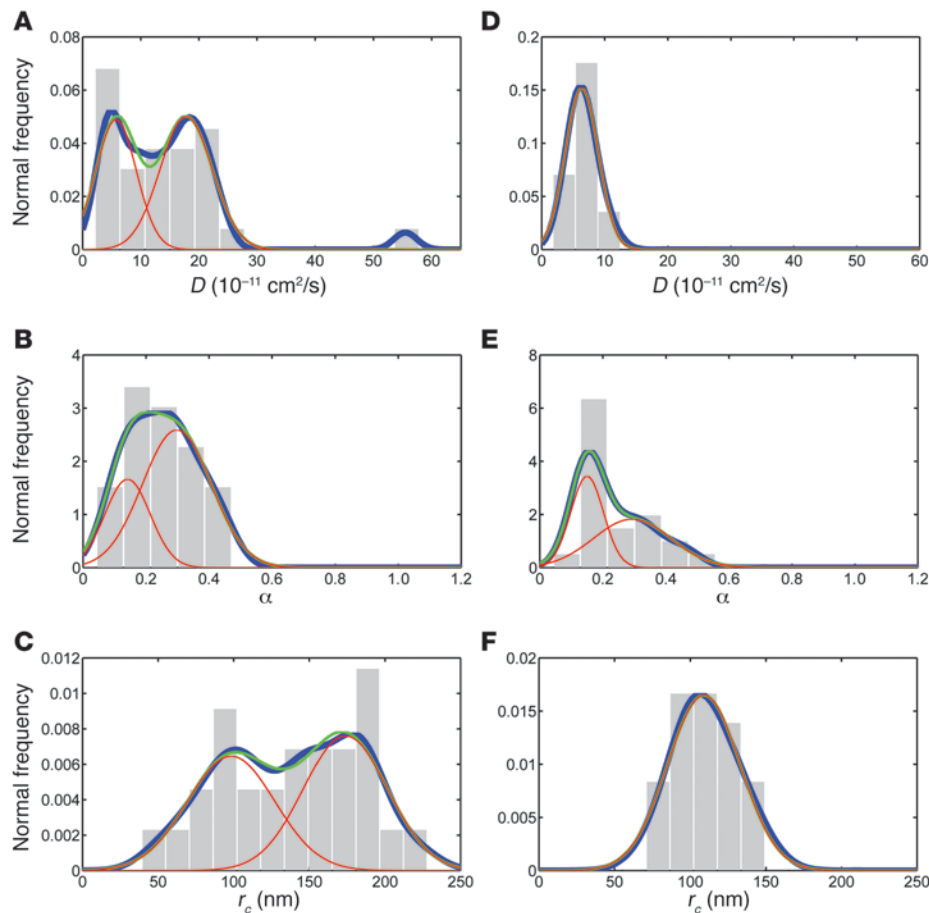
Figure 6
Distribution of band 3 diffusion parameters. The graphs in **A**–**C** represent normal rbc, and the graphs in **D**–**F** represent rbc with C3b deposits. In each graph, the gray bars represent a histogram of the experimental data; the blue curves represents the envelope smoothing function calculated from the experimental data; the red curves are Gaussian best-fit distributions, describing a single population (**D** and **F**) or 2 deconvolved populations (**A**–**C** and **E**); and the green curves are the sum of the red curves (see Methods). (**A**–**C** and **E**) The 2 red curves are normal distributions that differ statistically from one another according to Equation 2. D, diffusion coefficient; r_c, radius of confinement (see Methods).

from Sigma-Aldrich. Radioimmunoprecipitation (RIPA) buffer was from Upstate. HBSS and HBSS containing calcium and magnesium (HBSS++) were from Invitrogen/Gibco.

Monoclonal antibodies
Monoclonal mouse anti-human DAF (clone BRIC 216, IgG_1), anti-human band 3 (clone BRAC 17, IgG_{2b}), anti-human CD58 (clone BRIC 5, IgG_{2a}), and anti-human GPC (clone BRIC 10, IgG_1) were from International Blood Group Reference Laboratory (Bristol, United Kingdom). Monoclonal mouse anti-GPA (clone E4, IgM) was from Abcam. Monoclonal mouse anti-human C3dg (catalog no. A207, IgG_1) and monoclonal mouse anti-human C3c (catalog no. A205, IgG_1) were from Quidel. Monoclonal mouse anti-human C3b/iC3b (clone 8E11, IgG_1) and its hybridoma were provided by Ronald Taylor and William Sutherland (University of Virginia Medical School, Charlottesville, Virginia, USA) (51). Monoclonal mouse anti-fluorescein (clone 903, IgG_{2a}) was from Biodesign International. Fab fragments were prepared using the ImmunoPure Fab Preparation Kit (Pierce). The Fab fragment fraction was applied to a Protein A column (Pierce) to remove Fc fragments and any residual intact IgG. Fab preparations were dialyzed against PBS, pH 7.4, overnight. SDS-PAGE was used to confirm Fab purity.
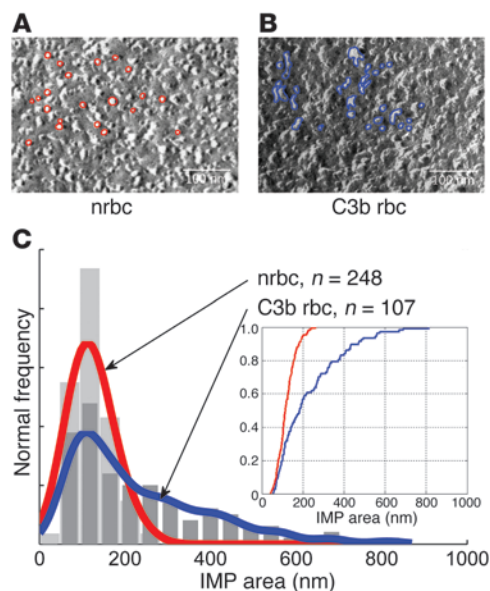
rbc with C3b deposits
rbc were obtained from normal donors after informed consent, according to human study protocols reviewed and approved by the institutional review boards at Harvard Medical School and Beth Israel Deaconess Medical Center. rbc (1×10^8) were washed twice in GVB++. A mixture of rbc, C5-depleted human serum (1:25 final dilution), and CVF (50 µg/ml) was

incubated in 200 µl (final volume) of GVB++, with 1 mM nickel chloride, for 20 minutes at 37°C. Controls for C3b deposition included rbc incubated with buffer alone and rbc incubated with C5-depleted human serum (1:25 final dilution) and CVF (50 µg/ml) in GVB++, with 5 mM EDTA.

Deposition of C3b/iC3b was confirmed by indirect immunofluorescence analysis using flow cytometry (FACScan; BD Biosciences — Immunocytometry Systems). For flow cytometry, 1×10^7 rbc with C3b deposits were resuspended in HEPES-buffered saline ([HBS] 16 mM HEPES, 137 mM NaCl, 3 mM KCl, pH 7.4), incubated with mouse anti-human C3c antibody (25 µg/ml) for 15 minutes at room temperature, washed twice in HBS, and incubated with FITC-conjugated goat anti-mouse antibody (25 µg/ml; Jackson ImmunoResearch Laboratories Inc.) for 15 minutes at room temperature. The mixture was then washed twice in HBS and resuspended in the same buffer at 1×10^7 cells/ml.

ELISA
rbc with C3b deposits (1×10^8) were washed twice in PBS and once in 5 mM phosphate and 140 mM NaCl, pH 8.0, and lysed in 1 ml of 5 mM phosphate, pH 8.0, with protease inhibitor cocktail (Complete, Mini, EDTA-free; Roche Diagnostics Corp.) for 20 minutes on ice. Ghosts were washed twice at 4°C in 1 ml of 5 mM phosphate, pH 8.0, and once at 4°C in 1 ml of PBS containing 1 mM $CaCl_2$ and resuspended to 80 µl (final volume) in PBS containing 1 mM $CaCl_2$ and 0.2% BSA. Twenty microliters of *Vibrio cholerae* neuraminidase (~0.2 U) was added to the cell suspension, and the mixture was incubated for 30 minutes at 37°C. After the incubation, 100 µl of 2% (final concentration) Triton X-100 with 0.2% BSA was added to the mixture. The cell extract was immediately used in an ELISA.

rbc labeling with conjugated gold particles

Blood from healthy donors was obtained with informed consent from the Hematology Laboratory at Brigham and Women's Hospital, Boston, Massachusetts, USA. EDTA was used as an anticoagulant. rbc counts were performed using the ADVIA 120 Hematology System (Bayer Corp.). rbc were washed 3 times with HBS, resuspended at 10% hematocrit in HBS with 10 mM glucose, and kept at 4°C until use. Alternatively, rbc were labeled with fluorescein thiosemicarbazide to derivatize cell-surface GPA (53). rbc (1×10^8) were washed twice in high-potassium PBS ([KPBS] 140 mM KCl, 15 mM Na_2HPO_4, pH 7.4), incubated with 1 mM $NaIO_4$ in 200 µl of KPBS for 15 minutes at 4°C, washed twice in 1 ml of KPBS with 0.1 M glycerol and once in KPBS, resuspended in 200 µl of KPBS, and mixed with 200 µl of 0.5 mg/ml fluorescein thiosemicarbazide in KPBS. The mixture was incubated for 1 hour at 4°C, washed 3 times in KPBS with 1% BSA, and kept at 4°C until use. Cells were typically used within 4–6 hours of phlebotomy. Immediately prior to SPT experiments, 20 µl of the cell suspension was incubated with 5 µl of the conjugated gold suspension for 40 minutes at room temperature. The mixture was then washed twice with 1 ml of HBS with 1% BSA.

Coimmunoprecipitation and mass spectrometry analysis of C3b-GPA complexes

rbc with C3b deposits and controls were prepared as described above. rbc were lysed in 1% NP-40 in PBS with 1:100 protease inhibitor cocktail (P8340; Sigma-Aldrich) for 30 minutes at 4°C and centrifuged at 5,600 *g* for 10 minutes. The supernatant was incubated with agarose beads coupled to either anti-C3dg monoclonal antibody or isotype-control antibody for 1 hour at 4°C. Anti-C3dg reacts with C3b as well as its processed forms iC3b and C3dg. Beads were washed 3 times in lysis buffer and twice in ice-cold PBS and were boiled in Laemmli nonreducing loading buffer. Proteins were separated by electrophoresis on 2 identical 3%–8% Tris-Acetate gels (Invitrogen). Proteins from the first gel were transferred onto nitrocellulose paper and developed with anti-GPA monoclonal antibody (5 µg/ml). The second gel was stained with Gel-Code Blue (Pierce), and the band corresponding to the GPA-positive area from the nitrocellulose paper was excised for mass spectrometry analysis.

Mass spectrometry. Protein bands from SDS-PAGE gels were digested with trypsin overnight at 37°C, pH 8.3, and the resulting peptide fragments were extracted from the gel bands. All collision-induced dissociation fragmentation data were acquired by C_{18} reversed phase microcapillary liquid chromatography, tandem mass spectrometry, using an ultra high resolution and mass accuracy Thermo Scientific Orbitrap XL Mass Spectrometer, operated in positive ion data-dependent acquisition mode. A Proxeon Biosystems EasynLC was used to deliver peptides at 300 nl/min over a 45-minute gradient. All tandem mass spectrometry spectra were analyzed using Sequest (revision 14; Thermo Scientific) and X! Tandem (www.thegpm.org; version 2007.01.01.1). X! Tandem was set up to search a subset of the Swiss-Prot database, assuming the digestion enzyme trypsin was used. Sequest was set up to search the concatenated reversed Swiss-Prot database (release 55.1; 619,242 forward entries). Sequest and X! Tandem were searched with a fragment ion mass tolerance of 1.00 Da and a parent ion tolerance of 0.20 Da. The iodoacetamide derivative of cysteine was specified in Sequest

ELISA wells were coated with anti-C3c antibody by incubation with 100 µl of the antibody (5 µg/ml) in 100 mM bicarbonate buffer, pH 8.1, at 4°C, overnight. The wells were washed once with PBS, incubated with 200 µl of 2% BSA in PBS for 1 hour at 37°C, and washed once with PBS. Fifty microliters of the previously prepared cell extract was then added to each well. After incubation for 1 hour at 37°C, wells were washed 3 times with washing buffer (PBS with 10 mM EDTA and 0.05% Tween-20) and incubated with 100 µl of biotinylated anti-C3b/iC3b antibody (5 µg/ml; prepared according to the manufacturer's instruction, using the EZ-Link NHS-PEO Solid Phase Biotinylation Kit: mini-spin columns; Pierce) for 1 hour at 37°C. The wells were washed 3 times with washing buffer, and 100 µl of avidin-biotin complex (Vector Laboratories) was added. The wells were then incubated for 1 hour at 37°C and washed 3 times with washing buffer. One hundred microliters of 2,2′-azino-di-(3-ethyl-benzthiazoline-6-sulphonic acid) solution (Zymed Laboratories) was added to each well, and the wells were incubated for 15 minutes at room temperature. The reactions were stopped by adding 100 µl of 0.1 M citric acid solution with 0.01% sodium azide. The plates were read at 415 nm in a microplate photometer. A standard curve was obtained using 10–500 ng/ml purified C3b (Advanced Research Technologies).

Conjugation of antibodies to gold particles

Gold particles were conjugated to Fab fragments as previously described (52). A mixture of specific Fab fragments and the nonspecific protein BSA was added to 0.5 ml of colloidal gold (~4.5×10^{10} particles) in 20 mM sodium phosphate buffer, pH 7.6. After 5 minutes of incubation at room temperature with constant shaking, BSA was added to a final concentration of 0.015% (w/v), and the mixture was incubated for another 10 minutes. After centrifugation at 10,000 *g* for 4 minutes at room temperature, the Fab-conjugated gold particles were resuspended in HBS with 0.03% BSA. The particles were then centrifuged at 10,000 *g* for 4 minutes at room temperature and the supernatant was discarded, leaving about 40 µl of gold colloid suspension ($OD_{530nm} \approx 5.0$, Cary 50 Bio UV-Visible Spectrophotometer; Varian Inc.). Fab-conjugated gold particles were maintained at 4°C and used within 24 hours. To minimize the possibility of crosslinking (i.e., a single particle conjugated to many specific Fab fragments), conjugation conditions were used such that 20%–40% of rbc in the sample were labeled with particles, and the labeled rbc had 1–5 particles per rbc (see below).
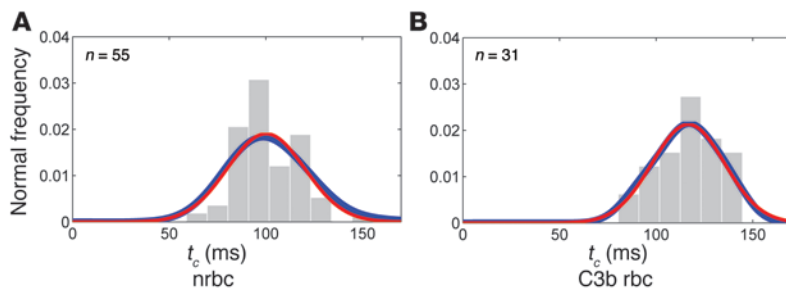
Figure 8
Probing rbc membrane viscoelastic properties by measuring time constant for rbc shape recovery after laser tweezers deformation. The shape recovery time constant depends on the shear modulus and surface viscosity of the rbc membrane (see Methods). For each panel, the blue curves represent the envelope smoothing function calculated from the experimental data (gray bars) and the red curves represent the Gaussian best-fit distribution of the envelope smoothing function. The difference between the distribution of shape recovery times for normal rbc (**A**; time constant [t_c] = 102 ± 2 ms) and rbc with C3b deposits (**B**; t_c = 117 ± 3 ms) was significant at P = 0.0001.

and X! Tandem as a fixed modification. Deamidation of asparagine and glutamine and oxidation of methionine were specified in Sequest and X! Tandem as variable modifications.

Criteria for protein identification. Scaffold (version Scaffold_2_00_03; Proteome Software Inc.) was used to validate tandem mass spectrometry–based peptide and protein identifications. Peptide identifications were accepted if they could be established at greater than 80.0% probability as specified by the Peptide Prophet algorithm (54). Protein identifications were accepted if they could be established at greater than 90.0% probability and contained at least 2 identified peptides. Protein probabilities were assigned by the Protein Prophet algorithm (55). Proteins that contained similar peptides and could not be differentiated based on tandem mass spectrometry analysis alone were grouped to satisfy the principles of parsimony.

FFEM of rbc membranes

rbc with C3b deposits were prepared as described above, fixed under mild conditions (0.5% glutaraldehyde for 30 minutes at 0°C), and stored at 0°C overnight. The samples were then prepared for FFEM by quenching, using the sandwich technique and liquid nitrogen-cooled propane (56). A cooling rate of 10,000°K per second was used to avoid ice crystal formation and cryofixation artifacts. The cryofixed samples were stored in liquid nitrogen for less than 2 hours before fracturing, which was performed using a JEOL JED-9000 freeze-etching apparatus. The exposed fracture planes were shadowed with platinum for 30 seconds at an angle of 25–35 degrees and with carbon for 35 seconds (2 kV/60–70 mA, 1×10^{-5} Torr). The replicas were cleaned with concentrated, fuming HNO_3 for 24 hours, repeatedly agitated with at least 5 changes of fresh chloroform/methanol (1:1 by volume), and examined on a JEOL 100 CX electron microscope.

Video microscopy and SPT

Gold particle-labeled rbc in HBS with 1% BSA were placed between a microscope slide and a coverslip. The coverslip was sealed with Cytoseal 60 Mounting Medium (Richard-Allan Scientific), and the system was equilibrated to 37°C for 15 minutes on a heating stage (Warner Instruments Corp.). A computer-enhanced differential interference contrast (DIC) microscopy was used to track the movement of the gold particles. We used an inverted microscope (Eclipse TE300; Nikon Instruments Inc.) equipped with an oil-immersion condenser and an oil-immersion

Plan-Apo objective (magnification, ×60; numerical aperture, 1.4). Illumination from a 100-W Mercury Arc Lamp (Osram Sylvania Ltd.) was guided through an Optical Fiber Scrambler (Technical Video). Images were recorded using a Photron FASTCAM PCI video camera (Photron USA Inc.) at a rate of 30 frames per second. The motion of individual gold particles was tracked for 20 seconds using MetaMorph (Universal Imaging Corp.), and the resulting trajectories were analyzed using custom routines written in the MATLAB environment (The MathWorks Inc.) and Mathematica (Wolfram Research Inc.).

Under DIC optics, a 40-nm gold particle was observed as a characteristic pattern on the rbc membrane. MetaMorph was used to determine the position of the intensity centroid of the gold particle pattern in each image frame. The algorithm of Gelles et al. (57) was used to track the intensity centroid from frame to frame, and the resulting time series of x and y coordinates was used for subsequent analyses. Tracks with more than 5% missing points (i.e., images in which the particle position could not be determined) were discarded. Observations were made only on cells with biconcave shapes.

Calculation of experimental parameters. The mean square displacement (MSD) of the gold particle was calculated, as follows, from the time series of x and y coordinates:

$$MSD(\Delta t_n) = \frac{1}{N-n} \sum_{i=1}^{N-n} [(x_{i+n} - x_i)^2 + (y_{i+n} - y_i)^2]$$

(Equation 1)

where x_i and y_i are the coordinates of the particle in the ith frame, $\Delta t_n = n \times \delta$, n is an integer between 1 and N, δ is the time interval between successive frames (δ = 33 ms for images recorded at 30 frames per second), and N is the total number of frames (58).

The lateral diffusion coefficient, D, of the gold particle was estimated from the initial slope of the MSD versus Δt relationship, i.e., by fitting a straight line to the MSD calculated at Δt_1, Δt_2, Δt_3, and Δt_4. The time-dependence factor, α, for 2-dimensional diffusion that describes the overall degree of confinement of the gold particle was estimated from $MSD = 4D_{traj}t^\alpha$, where D_{traj} is the trajectory-averaged diffusion coefficient and t denotes time.

Theoretically, Brownian motion is characterized by a time-dependence factor of 1, whereas confined motion has time-dependence factor values of less than 1 and directed motion have time-dependence factor values of more than 1 (59). For confined motion, the MSD plot approaches an asymptote at the value $MSD(t \to \infty) = r_c^2$, where r_c is the radius of confinement. The radius of confinement was obtained by fitting experimental MSD values to the MSD of a particle trapped in a circular confinement, expanded to the second term of the Bessel function (60): $MSD = r_c^2 [1 - 0.994\exp(-3.39D_{traj}t/r_c^2) - 0.0104\exp(-28.4D_{traj}t/r_c^2)]$.

Diffusion trajectories were classified as tightly confined or loosely confined or Brownian based on the population analysis described by Cairo et al. (61). Briefly, a kernel-smoothing probability density calculation was used to smooth the normalized distribution of time-dependence factor values for each experimental condition. This envelope (smoothing) curve was then fitted to the sum of 2 Gaussian distributions, which represented 2 populations of diffusion trajectories. The 2 Gaussian distributions had independent means and standard deviations. According to Johnson et al. (62), the following equation was used to find out if 2 normal distributions are statistically different:

$$\frac{\sigma_1^2 + \sigma_2^2}{\sigma_1^2 \sigma_2^2} (\mu_1 - \mu_2)^2 > 8$$
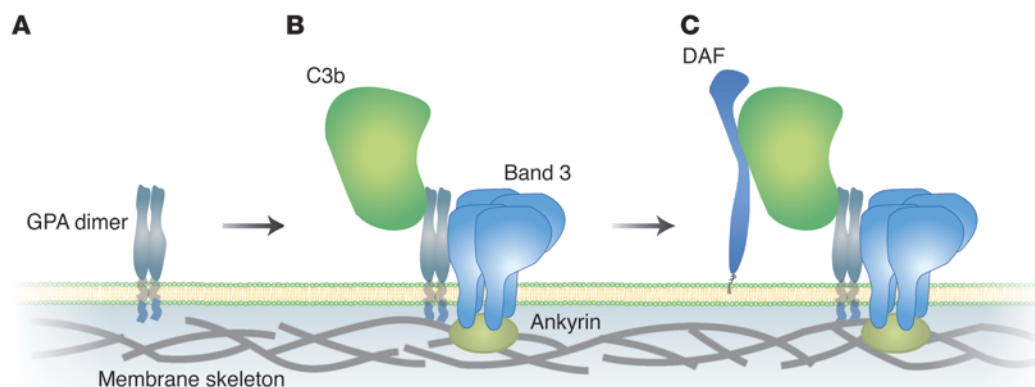
(Equation 2)

Figure 9
Working model for the interaction of DAF, C3b, GPA, band 3, and the rbc membrane skeleton. (**A**) Complement activation causes the generation of C3b, which binds predominantly to GPA dimers. (**B**) C3b binding to GPA stimulates formation of a C3b-GPA–band 3 complex that is linked to the spectrin-based membrane skeleton via ankyrin. (**C**) DAF becomes immobilized through its interaction with C3b-GPA. DAF structure was obtained from Lukacik et al. (6). The diagram is approximate in scale. It should be noted that the GPA and band 3 molecules shown in the figure represent only approximately 0.1% of the total GPA and band 3 molecules in the rbc membrane. Since binding of approximately 2,000 C3b molecules to GPA induces immobilization of approximately 50,000 GPA and band 3 oligomers in the rbc membrane, we suggest that GPA ligation by C3b and C3b-linked protein complex formation causes secondary membrane skeletal changes that result in immobilization of a much larger fraction of GPA and band 3 molecules than those molecules involved directly in the C3b-linked membrane protein complex.

where μ and σ denote the mean and SD of each distribution, respectively. Trajectories with time-dependence factor values falling under the Gaussian curve with the lower mean were classified as tightly confined, and trajectories with time-dependence factor values falling under the Gaussian curve with the higher mean were classified as loosely confined or Brownian. The fractional percentage of each population was calculated from the normalized weighting factor, by which each Gaussian distribution was multiplied in the best-fitted sum. The average diffusion coefficient of each population and the average radius of confinement of each tightly confined population was calculated for the trajectories classified as tightly confined or loosely confined or Brownian by the criteria listed above.

LOT
Polystyrene particle conjugation. Monoclonal antibody directed against DAF or fluorescein (to label cell-surface GPA derivatized with fluorescein thiosemicarbazide) was covalently attached to 1-μm polystyrene particles with carboxyl surfaces (Polysciences Inc.). Particles (~9.1 × 10⁸) were washed twice in 1 ml of MES buffer, pH 6.1. For each wash, the mixture was sonicated for 5 minutes and centrifuged at 8,000 *g* for 5 minutes, and the particles were resuspended in 50 μl of MES buffer. The carboxyl groups on the particles were sensitized by incubating the particle mixture in 100 μl (final volume) of 100 mM *N*-hydroxysuccinimide and 0.4% 1-ethyl-3-(3-dimethylaminopropyl) carbodiimide hydrochloride for 20 minutes at room temperature. The mixture was then washed twice in 1 ml of MES buffer and resuspended in 50 μl of MES buffer. Ten microliters of antibody (5 μg/ml) was added to the particle suspension and the mixture was incubated with constant shaking for 2 hours at room temperature. BSA was then added to 1% (final concentration) and the mixture was incubated for 15 minutes. The conjugation reaction was terminated by adding ethanolamine to 100 mM final concentration and the incubation was continued for another 15 minutes. The mixture was then washed twice in HBS with 0.1% BSA. Using this protocol, 20%–40% of rbc in the sample were labeled with particles, and the labeled rbc had 1–3 particles per rbc. The conjugated particles were stored at 4°C and used within 1 week.

Sample preparation. About 1 × 10⁷ rbc in 20 μl of HBS with 1% BSA were incubated with 5 μl of the polystyrene particle preparation for 20 minutes at room temperature. Labeled rbc were washed once in 1 ml of PBS with 1% BSA and then resuspended in 200 μl of PBS. Ten microliters of the mixture was placed between a microscope slide and a coverslip, and the coverslip was sealed with Cytoseal 60 Mounting Medium.

Tether-pulling experiment. The rbc sample was placed on an Eclipse TE300 inverted microscope (Nikon) equipped with an oil-immersion condenser and an oil-immersion Plan-NEOFLUAR objective (magnification, ×100; numerical aperture, 1.3 (Zeiss). The light source for LOT was a 1,064-nm Nd:YVO₄ laser (Spectra Physics Lasers), lasing at 1 W. Calibration experiments showed that the LOT stiffness was 5.5 μN/m. A trapped particle was gradually pulled away from the rbc membrane by translating the sample stage at a constant velocity of 10 μm/min. The presence or absence of a lipid tether was recorded after 5 μm of stage translation.

Deformation of rbc and shape recovery time. Anti-GPC antibody was covalently attached to 1-μm polystyrene particles essentially as described above, except that a 20-fold higher concentration of antibody was used. Thus, the bead would have been attached to the cell by multiple antibody-antigen bonds, thereby providing us with a multivalent "handle" to use with LOT. rbc were mixed with beads in HBS with 5% BSA and placed between 2 glass coverslips to make a 30-μm thick sample. Most of the rbc attached to the glass at a small area on the rim. The LOT was used to trap a bead from the solution, bring the trapped bead into contact with a rbc for 5 seconds (which usually resulted in strong attachment), and then translate the trapped bead by 2 μm, at a rate of 20 μm/min, to extend the cell into an elliptical shape. Upon switching off the LOT, the bead was released and the rbc recovered its circular (discocytic) shape. The bead position was recorded at 30 frames per second. The first 0.5 seconds of each trajectory were fitted by an exponent with recovery time constant t_c. Hochmuth et al. (27) have estimated that the characteristic time for relaxation is given by $t_c = \eta/\mu$, where η is the surface viscosity of the rbc membrane and μ is the shear modulus of the membrane.

Statistics
The nonparametric 1-way Kruskal-Wallis test (63) was performed in MATLAB. The Kruskal-Wallis method was preferred because of its resistance to outliers. *P* values of less than 0.05 were considered to be significant.

Address correspondence to: David E. Golan, Department of Biological Chemistry and Molecular Pharmacology, Harvard Medical School, 250 Longwood Avenue, SGMB 304, Boston, Massachusetts 02115, USA. Phone: (617) 432-2256; Fax: (617) 432-3833; E-mail: dgolan@hms.harvard.edu.

Pallop Karnchanaphanurach's present address is: Department of Chemistry, Center of Excellence for Innovation in Chemistry and Center for Alternative Energy, Faculty of Science, Mahidol University, Bangkok, Thailand.

1. Nicholson-Weller, A. 2007. Complement. In *Endothelial biomedicine*. W. Aird, editor. Cambridge University Press. New York, New York, USA. 430–443.
2. Michaels, D.W., Abramovitz, A.S., Hammer, C.H., and Mayer, M.M. 1976. Increased ion permeability of planar lipid bilayer membranes after treatment with the C5b-9 cytolytic attack mechanism of complement. *Proc. Natl. Acad. Sci. U. S. A.* **73**:2852–2856.
3. Nicholson-Weller, A., Burge, J., Fearon, D.T., Weller, P.F., and Austen, K.F. 1982. Isolation of a human erythrocyte membrane glycoprotein with decay-accelerating activity for C3 convertases of the complement system. *J. Immunol.* **129**:184–189.
4. Caras, I.W., et al. 1987. Cloning of decay-accelerating factor suggests novel use of splicing to generate two proteins. *Nature.* **325**:545–549.
5. Medof, M.E., et al. 1987. Cloning and characterization of cDNAs encoding the complete sequence of decay-accelerating factor of human complement. *Proc. Natl. Acad. Sci. U. S. A.* **84**:2007–2011.
6. Lukacik, P., et al. 2004. Complement regulation at the molecular level: the structure of decay-accelerating factor. *Proc. Natl. Acad. Sci. U. S. A.* **101**:1279–1284.
7. Medof, M.E., Kinoshita, T., and Nussenzweig, V. 1984. Inhibition of complement activation on the surface of cells after incorporation of decay-accelerating factor (DAF) into their membranes. *J. Exp. Med.* **160**:1558–1121.
8. Roberts, W.N., et al. 1985. Normal function of CR1 on affected erythrocytes of patients with paroxysmal nocturnal hemoglobinuria. *J. Immunol.* **134**:512–517.
9. Fujita, T., Inoue, T., Ogawa, K., Iida, K., and Tamura, N. 1987. The mechanism of action of decay-accelerating factor (DAF). DAF inhibits the assembly of C3 convertases by dissociating C2a and Bb. *J. Exp. Med.* **166**:1221–1228.
10. Hourcade, D.E., Mitchell, L., Kuttner-Kondo, L.A., Atkinson, J.P., and Medof, M.E. 2002. Decay-accelerating factor (DAF), complement receptor 1 (CR1), and factor H dissociate the complement AP C3 convertase (C3bBb) via sites on the type A domain of Bb. *J. Biol. Chem.* **277**:1107–1112.
11. Kuttner-Kondo, L.A., et al. 2003. A corresponding tyrosine residue in the C2/factor B type A domain is a hot spot in the decay acceleration of the complement C3 convertases. *J. Biol. Chem.* **278**:52386–52391.
12. Kinoshita, T., Medof, M.E., and Nussenzweig, V. 1986. Endogenous association of decay-accelerating factor (DAF) with C4b and C3b on cell membranes. *J. Immunol.* **136**:3390–3395.
13. Pangburn, M.K., Pangburn, K.L., Koistinen, V., Meri, S., and Sharma, A.K. 2000. Molecular mechanisms of target recognition in an innate immune system: interactions among factor H, C3b, and target in the alternative pathway of human complement. *J. Immunol.* **164**:4742–4751.
14. Parker, C.J., Soldato, C.M., and Rosse, W.F. 1984. Abnormality of glycophorin-alpha on paroxysmal nocturnal hemoglobinuria erythrocytes. *J. Clin. Invest.* **73**:1130–1143.
15. Ninomiya, H., Abe, T., Shichishima, T., Terasawa, T., and Fujita, T. 1988. Decay-accelerating factor (DAF) on the blood cell membranes in patients with paroxysmal nocturnal haemoglobinuria (PNH): measurement by enzyme-linked immunosorbent assay (ELISA). *Br. J. Haematol.* **69**:81–87.
16. Lutz, H.U. 1999. How pre-existing, germline-derived antibodies and complement may help induce a primary immune response to nonself. *Scand J. Immunol.* **49**:224–228.
17. Dustin, M.L., Sanders, M.E., Shaw, S., and Springer, T.A. 1987. Purified lymphocyte function-associated antigen 3 binds to CD2 and mediates T lymphocyte adhesion. *J. Exp. Med.* **165**:677–692.
18. Chasis, J.A., Mohandas, N., and Shohet, S.B. 1985. Erythrocyte membrane rigidity induced by glycophorin A-ligand interaction. Evidence for a ligand-induced association between glycophorin A and skeletal proteins. *J. Clin. Invest.* **75**:1919–1926.
19. Chasis, J.A., Reid, M.E., Jensen, R.H., and Mohandas, N. 1988. Signal transduction by glycophorin A: role of extracellular and cytoplasmic domains in a modulatable process. *J. Cell Biol.* **107**:1351–1357.
20. Knowles, D.W., Chasis, J.A., Evans, E.A., and Mohandas, N. 1994. Cooperative action between band 3 and glycophorin A in human erythrocytes: immobilization of band 3 induced by antibodies to glycophorin A. *Biophys. J.* **66**:1726–1732.
21. Bennett, V. 1989. The spectrin-actin junction of erythrocyte membrane skeletons. *Biochim. Biophys. Acta.* **988**:107–121.
22. Tomita, M., Furthmayr, H., and Marchesi, V.T. 1978. Primary structure of human erythrocyte glycophorin A. Isolation and characterization of peptides and complete amino acid sequence. *Biochemistry.* **17**:4756–4770.
23. Liu, S.C., et al. 1995. Molecular basis of altered red blood cell membrane properties in Southeast Asian ovalocytosis: role of the mutant band 3 protein in band 3 oligomerization and retention by the membrane skeleton. *Blood.* **86**:349–358.
24. Golan, D.E., Alecio, M.R., Veatch, W.R., and Rando, R.R. 1984. Lateral mobility of phospholipid and cholesterol in the human erythrocyte membrane: effects of protein-lipid interactions. *Biochemistry.* **23**:332–339.
25. Sung, K.L., Freedman, J., Chabanel, A., and Chien, S. 1985. Effect of complement on the viscoelastic properties of human erythrocyte membrane. *Br. J. Haematol.* **61**:455–466.
26. Sutera, S.P., et al. 1985. Age-related changes in deformability of human erythrocytes. *Blood.* **65**:275–282.
27. Hochmuth, R.M., Worthy, P.R., and Evans, E.A. 1979. Red cell extensional recovery and the determination of membrane viscosity. *Biophys. J.* **26**:101–114.
28. Waugh, R.E., et al. 1992. Rheologic properties of senescent erythrocytes: loss of surface area and volume with red blood cell age. *Blood.* **79**:1351–1358.
29. Lublin, D.M., and Coyne, K.E. 1991. Phospholipid-anchored and transmembrane versions of either decay-accelerating factor or membrane cofactor protein show equal efficiency in protection from complement-mediated cell damage. *J. Exp. Med.* **174**:35–44.
30. Zhang, F., et al. 1991. Lateral diffusion of membrane-spanning and glycosylphosphatidylinositol-linked proteins: toward establishing rules governing the lateral mobility of membrane proteins. *J. Cell Biol.* **115**:75–84.
31. Pangburn, M.K. 1986. Differences between the binding sites of the complement regulatory proteins DAF, CR1, and factor H on C3 convertases. *J. Immunol.* **136**:2216–2221.
32. Marchesi, V.T., Furthmayr, H., and Tomita, M. 1976. The red cell membrane. *Annu. Rev. Biochem.* **45**:667–698.
33. Parker, C.J., Soldato, C.M., and Telen, M.J. 1984. Increased efficiency of binding of nascent C3b to the erythrocytes of chronic cold agglutinin disease. *J. Clin. Invest.* **74**:1050–1062.
34. Craig, M.L., Waitumbi, J.N., and Taylor, R.P. 2005. Processing of C3b-opsonized immune complexes bound to non-complement receptor 1 (CR1) sites on red cells: phagocytosis, transfer, and associations with CR1. *J. Immunol.* **174**:3059–3066.
35. Hochmuth, R.M., and Waugh, R.E. 1987. Erythrocyte membrane elasticity and viscosity. *Annu. Rev. Physiol.* **49**:209–219.
36. Bronkhorst, P.J., et al. 1995. A new method to study shape recovery of red blood cells using multiple optical trapping. *Biophys. J.* **69**:1666–1673.
37. Henon, S., Lenormand, G., Richert, A., and Gallet, F. 1999. A new determination of the shear modulus of the human erythrocyte membrane using optical tweezers. *Biophys. J.* **76**:1145–1151.
38. Chien, S., Sung, K.L., Skalak, R., Usami, S., and Tozeren, A. 1978. Theoretical and experimental studies on viscoelastic properties of erythrocyte membrane. *Biophys. J.* **24**:463–487.
39. Mills, J.P., Qie, L., Dao, M., Lim, C.T., and Suresh, S. 2004. Nonlinear elastic and viscoelastic deformation of the human red blood cell with optical tweezers. *Mech. Chem. Biosyst.* **1**:169–180.
40. Linderkamp, O., and Meiselman, H.J. 1982. Geometric, osmotic, and membrane mechanical properties of density- separated human red cells. *Blood.* **59**:1121–1127.
41. Piomelli, S., and Seaman, C. 1993. Mechanism of red blood cell aging: relationship of cell density and cell age. *Am. J. Hematol.* **42**:46–52.
42. Aminoff, D. 1988. The role of sialoglycoconjugates in the aging and sequestration of red cells from circulation. *Blood Cells.* **14**:229–257.
43. Jain, S.K., Mohandas, N., Clark, M.R., and Shohet, S.B. 1983. The effect of malonyldialdehyde, a product of lipid peroxidation, on the deformability, dehydration and 51Cr-survival of erythrocytes. *Br. J. Haematol.* **53**:247–255.
44. Connor, J., Pak, C.C., and Schroit, A.J. 1994. Exposure of phosphatidylserine in the outer leaflet of human red blood cells. Relationship to cell density, cell age, and clearance by mononuclear cells. *J. Biol. Chem.* **269**:2399–2404.
45. Schroit, A.J., Madsen, J.W., and Tanaka, Y. 1985. In vivo recognition and clearance of red blood cells containing phosphatidylserine in their plasma membranes. *J. Biol. Chem.* **260**:5131–5138.
46. Kay, M. 2005. Immunoregulation of cellular life span.

Ann. N. Y. Acad. Sci. **1057**:85–111.

47. Kay, M.M. 2004. Band 3 and its alterations in health and disease. *Cell. Mol. Biol. (Noisy-le-grand)*. **50**:117–138.

48. Turrini, F., Mannu, F., Arese, P., Yuan, J., and Low, P.S. 1993. Characterization of the autologous antibodies that opsonize erythrocytes with clustered integral membrane proteins. *Blood*. **81**:3146–3152.

49. Lutz, H.U., Stammler, P., and Fasler, S. 1993. Preferential formation of C3b-IgG complexes in vitro and in vivo from nascent C3b and naturally occurring anti-band 3 antibodies. *J. Biol. Chem.* **268**:17418–17426.

50. Freedman, J. 1984. Membrane-bound immunoglobulins and complement components on young and old red cells. *Transfusion*. **24**:477–481.

51. Tosic, L., Sutherland, W.M., Kurek, J., Edberg, J.C., and Taylor, R.P. 1989. Preparation of monoclonal antibodies to C3b by immunization with C3b(i)-sepharose. *J. Immunol. Methods*. **120**:241–249.

52. Mirchev, R., and Golan, D.E. 2001. Single-particle tracking and laser optical tweezers studies of the dynamics of individual protein molecules in membranes of intact human and mouse red cells. *Blood Cells Mol. Dis.* **27**:143–147.

53. Corbett, J.D., and Golan, D.E. 1993. Band 3 and glycophorin are progressively aggregated in density-fractionated sickle and normal red blood cells. Evidence from rotational and lateral mobility studies. *J. Clin. Invest.* **91**:208–217.

54. Keller, A., Nesvizhskii, A.I., Kolker, E., and Aebersold, R. 2002. Empirical statistical model to estimate the accuracy of peptide identifications made by MS/MS and database search. *Anal. Chem.* **74**:5383–5392.

55. Nesvizhskii, A.I., Keller, A., Kolker, E., and Aebersold, R. 2003. A statistical model for identifying proteins by tandem mass spectrometry. *Anal. Chem.* **75**:4646–4658.

56. Sternberg, B. 1993. Freeze-fracture electron microscopy of liposomes. In *Liposome preparation and related techniques*. G. Gregoriadis, editor. CRC Press. Boca Raton, Florida, USA. 363–383.

57. Gelles, J., Schnapp, B.J., and Sheetz, M.P. 1988. Tracking kinesin-driven movements with nanometre-scale precision. *Nature*. **331**:450–453.

58. Qian, H., Sheetz, M.P., and Elson, E.L. 1991. Single particle tracking. Analysis of diffusion and flow in two-dimensional systems. *Biophys. J.* **60**:910–921.

59. Saxton, M.J., and Jacobson, K. 1997. Single-particle tracking: applications to membrane dynamics. *Annu. Rev. Biophys. Biomol. Struct.* **26**:373–399.

60. Saxton, M.J. 1993. Lateral diffusion in an archipelago. Single-particle diffusion. *Biophys. J.* **64**:1766–1780.

61. Cairo, C.W., Mirchev, R., and Golan, D.E. 2006. Cytoskeletal regulation couples LFA-1 conformational changes to receptor lateral mobility and clustering. *Immunity*. **25**:297–308.

62. Johnson, N.L., Kotz, S., and Balakrishnan, N. 1994. *Continuous univariate distributions*. John Wiley. New York, New York, USA. 756 pp.

63. Hollander, M., and Wolfe, D.A. 1999. *Nonparametric statistical methods*. John Wiley. New York, New York, USA. 787 pp.